Neutron powder diffraction and Mössbauer spectroscopy (119Sn and 155Gd) studies of the CeScSi-type GdMgSn and GdMgPb compounds

P. Lemoine, Nicolas R. Lee-Hone, D. H. Ryan, A. Vernière, Bernard Malaman, Gérard Le Caër

Neutron powder diffraction and Mössbauer spectroscopy (^{119}Sn and ^{155}Gd) studies of the CeScSi-type GdMgSn and GdMgPb compounds

P. Lemoine*

Department of Physics and Astronomy, University of Manitoba, Winnipeg, Manitoba, Canada R3T 2N2 and Institut Jean Lamour, Département P2M, équipe 103, CNRS (UMR 7198), Faculté des Sciences et Technologies, Université de Lorraine, Boîte Postale 70239, 54506 Vandœuvre-lès-Nancy Cedex, France

N. R. Lee-Hone† and D. H. Ryan

Physics Department and Centre for the Physics of Materials, McGill University, 3600 University Street, Montreal, Quebec, Canada H3A 2T8

A. Vernière and B. Malaman

Institut Jean Lamour, Département P2M, équipe 103, CNRS (UMR 7198), Faculté des Sciences et Technologies, Université de Lorraine, Boîte Postale 70239, 54506 Vandœuvre-lès-Nancy Cedex, France

G. Le Caër

Institut de Physique de Rennes, UMR UR1–CNRS 6251, Université de Rennes I, Campus de Beaulieu, 35042 Rennes Cedex, France

The magnetic structures of the CeScSi-type GdMgSn and GdMgPb compounds have been studied by both neutron powder diffraction and Mössbauer spectroscopy (^{119}Sn and ^{155}Gd). The neutron diffraction results show that the two compounds adopt incommensurate antiferromagnetic structures at 5.4 K with propagation vectors $\vec{k} = [0.910, 0.077, 0]$ for GdMgSn and $\vec{k} = [0.892, 0, 0]$ for GdMgPb. The magnetic moments lie in the basal plane, which is confirmed by both ^{119}Sn and ^{155}Gd Mössbauer spectroscopy. Mössbauer spectroscopy refinements and simulations reveal that the magnetic structure of GdMgSn is cycloidal at low temperature and undergoes a transition to a modulated magnetic structure above $T \sim 40$ K. A similar magnetic transition is inferred for GdMgPb. The magnetic structures of GdMgSn and GdMgPb are compared with those of other CeScSi-type compounds.

PACS number(s): 75.25.−j, 61.05.fm, 76.80.+y

I. INTRODUCTION

The *R*MgSn and *R*MgPb compounds (where *R* is a rare-earth element) crystallize in the CeScSi-type structure (space group $I4/mmm$, No. 139) [1–3] and order antiferromagnetically with T_N ranging from 2.5 K for TmMgPb to 79 K for SmMgSn [3,4]. A few other compounds in the *RTX* series (where *T* is a transition metal and *X* is a *p*-block element) such as PrScSi [5], PrScGe [5,6], and ErZrSb [7] are antiferromagnetic at low temperatures, while most CeScSi-type compounds are ferromagnetic at low temperatures: *R*ScSi (R = Ce,Nd,Sm,Gd) [5,8–10], *R*ScGe (R = Ce − Nd,Sm,Gd,Tb) [5,6,8–14], *R*ZrSb (R = Gd − Tm) [7,15], and *R*TiGe (R = Gd,Tb) [16–20].

Neutron powder diffraction studies on the CeScSi-type *R*MgSn and *R*MgPb compounds [4,21,22] have revealed relatively complex magnetic structures with similar magnetic arrangements for any given rare-earth element. For example, at very low temperatures PrMgSn, PrMgPb, NdMgSn, and NdMgPb each adopt commensurate antiferromagnetic structures, TbMgSn and TbMgPb adopt incommensurate sine-wave-modulated magnetic structures, and DyMgSn, DyMgPb, HoMgSn, HoMgPb, ErMgSn, and ErMgPb adopt square-wave-modulated magnetic structures [4,22]. The only exception to this consistency seems to be between the TmMgSn/TmMgPb pair. TmMgSn adopts a square-wave-modulated magnetic structure while TmMgPb adopts a more complicated magnetic structure with two propagation vectors [4,22].

Mössbauer spectroscopy and neutron diffraction play complementary roles in the study of magnetic order in rare-earth intermetallics. The first provides local information on magnetic environments, while the second yields values for ordered moments and a description of the long-range magnetic order [23]. We have therefore used these techniques to complete the magnetic structure characterization of the CeScSi-type *R*MgSn and *R*MgPb series by studying the antiferromagnetic structure of GdMgSn and GdMgPb ($T_N = 48(2)$ K and 47(2) K, respectively) [3,4]. We performed ^{119}Sn and ^{155}Gd Mössbauer spectroscopy and neutron powder diffraction using a large-area flat-plate-geometry sample holder [24,25]. The flat-plate sample holder allows one to obtain diffraction patterns of intermetallic compounds with high thermal neutron absorption cross-section elements (Sm, Eu, Gd, Cd, B), without resorting to short wavelengths or isotopically enriched samples. This technique has been used successfully in many recent studies [26–31].

II. EXPERIMENTAL METHODS

The polycrystalline samples were synthesized starting from stoichiometric amounts of high-purity commercially available elements (99.9 wt % for lead and gadolinium, 99.99 wt %

*pierric.lemoine@ensicaen.fr
†nicholas.lee-hone@mail.mcgill.ca

for magnesium and tin). As a general precaution, all sample manipulations were undertaken in a purified argon-filled glovebox ensuring an oxygen level of less than 2 ppm O_2 and about 3 ppm H_2O. Due to the high volatility of magnesium, the elements were placed in an arc-welded Mo crucible. The elements were then melted in a water-cooled copper crucible using a high-frequency induction furnace (CELES), under secondary vacuum. To prevent oxidation, the Mo crucibles were subsequently enclosed in a silica tube under purified argon (300 mm Hg), placed in a furnace for two weeks at 1073 K, and then water cooled. There was no noticeable reaction between the samples and the container.

The crystallographic structure and presence of impurities were checked by x-ray powder diffraction (Philips X'Pert Pro Diffractometer, Cu $K\alpha$). The analysis of the patterns was performed by Rietveld profile refinement using the FULLPROF/WINPLOTR suite [32,33]. It is worth noting that at this stage, the samples were clearly observed to deteriorate in air, justifying the precautions taken during sample preparation.

Thermal neutron diffraction experiments were carried out on the C2 multiwire powder diffractometer (DUALSPEC) at the NRU reactor, Canadian Neutron Beam Centre, Chalk River, Ontario. A large-area silicon flat-plate sample holder [24,25] was used to minimize the effects of absorption by the natural Gd in the sample. Most of the data were taken at a neutron wavelength of $\lambda = 1.3286(1)$ Å to make best use of the available flux from the thermal source. However, a set of diffraction patterns was also obtained at the longer wavelength of $\lambda = 2.3731(1)$ Å to ensure that no low-q magnetic diffraction peaks were being lost in the direct beam at $\lambda = 1.3286(1)$ Å. Temperatures down to 5.4 K were obtained using a closed-cycle fridge. As the samples are air sensitive, they were ground and mounted in the flat-plate sample holder under a helium atmosphere and then sealed into an aluminum can to guarantee a helium atmosphere at all times during transport and measurement. These materials blacken quite rapidly on exposure to air but when the samples were removed from the mounts several months after the measurements, no such discoloration was observed. All full-pattern magnetic and structural refinements employed the FULLPROF/WINPLOTR suite [32,33] with neutron scattering length coefficients for natural Gd taken from the tabulation by Lynn and Seeger [34]. No absorption correction was applied; however, the data were truncated at $2\theta = 52.5^\circ$ to minimize the impact of angle-dependent absorption effects.

For the ^{155}Gd Mössbauer spectroscopy measurements, the sample and 50 mCi $^{155}SmPd_3$ source were mounted vertically in a helium flow cryostat, and the drive was operated in sine mode. The drive system was calibrated using a laser interferometer with velocities cross-checked against both ^{57}Co**Rh**/α-Fe at room temperature and $GdFe_2$ at 5 K. The spectra were fitted using a nonlinear least-squares minimization routine with line positions and intensities derived from an exact solution to the full Hamiltonian [35].

^{119}Sn Mössbauer spectra were collected in transmission mode on a constant-acceleration spectrometer using a ~10 mCi $Ba^{119m}SnO_3$ source with the sample in a helium flow cryostat. The source was kept at room temperature. A 25 μm Pd foil was used to absorb the Sn $K\alpha$ x rays also emitted by the source. The spectrometer was calibrated with a 25 mCi ^{57}Co**Rh** source and α-Fe at room temperature, and the ^{119}Sn isomer shifts are referenced to $BaSnO_3$ at room temperature. Mössbauer spectra that have no hyperfine field distribution were fitted with a standard least-squares method assuming Lorentzian peaks. The magnetically split spectra that have a distribution of hyperfine fields were analyzed by a constrained Hesse-Rübartsch method as described in Ref. [36]. This method extracts a hyperfine magnetic field distribution $P(B)$ from an experimental spectrum, where $P(B)\Delta B$ represents the fraction of tin atoms whose field is between B and $B + \Delta B$. To obtain $P(B)$ ($\geqslant 0$), the spectrum is considered to be a sum of N sextets of Lorentzian lines with a full width at half maximum Γ of 0.6 mm/s, characteristic of the ^{119}Sn isotope. The calculated distribution is thus a histogram of N bins of identical widths $\Delta B \sim 0.15-0.20$ T. It is normalized so that $\sum_{i=1}^{N} P(B_i)\Delta B = 1$, with $B_i = (i - 1/2)\Delta B$ ($i = 1, \ldots, N$).

III. RESULTS AND DISCUSSION

The neutron powder diffraction patterns taken at 60 and 5.4 K, along with the difference between these patterns, are shown in Fig. 1. The appearance of purely magnetic peaks

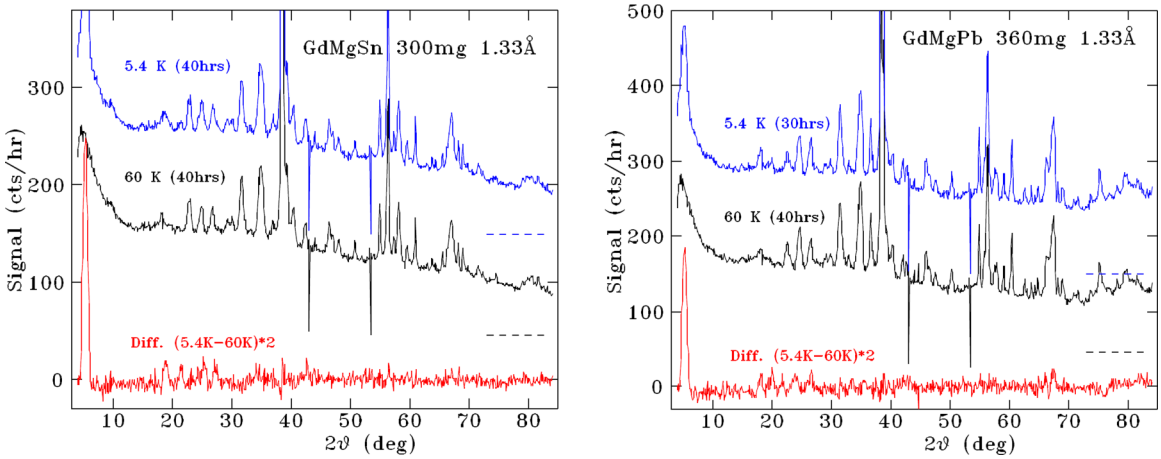

FIG. 1. (Color online) Neutron diffraction patterns of GdMgSn (left) and GdMgPb (right) at 60 and 5.4 K, together with the difference between the two patterns. The 60 and 5.4 K patterns have been offset vertically for clarity and their respective baseline positions are shown by the dashed lines at the right.

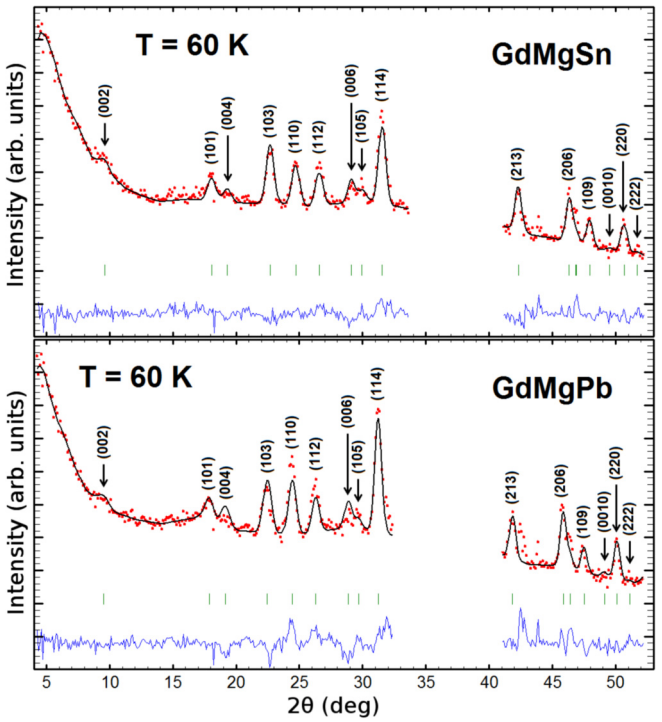

FIG. 2. (Color online) Refinement of the neutron diffraction patterns of GdMgSn and GdMgPb in the paramagnetic state with $\lambda = 1.3286(1)$ Å.

at low temperature in the angular range $4^\circ \leqslant 2\theta \leqslant 28^\circ$ is clearly observed, confirming the antiferromagnetic order of these compounds.

A. Paramagnetic neutron diffraction

The neutron powder diffraction patterns recorded in the paramagnetic state ($T = 60$ K) clearly show the nuclear Bragg peaks of the CeScSi-type GdMgSn and GdMgPb compounds (Fig. 2). Extra diffraction peaks due to the sample mount were observed in the $2\theta = 34^\circ - 41^\circ$ range, so this entire region was excluded from the refinements. The crystallographic data obtained from the refinements of the 60 K neutron diffraction patterns are presented in Table I. The GdMgX (X = Sn,Pb) compounds crystallize in the tetragonal space group $I4/mmm$. In this structure the Gd, Mg, and X atoms

TABLE I. Crystallographic data of GdMgSn and GdMgPb obtained by refinement of the 60 K neutron powder diffraction patterns with $\lambda = 1.3286(1)$ Å.

	GdMgSn	GdMgPb
a (Å)	4.391(4)	4.437(4)
c (Å)	15.855(14)	15.984(18)
z_{Gd}	0.341(1)	0.344(1)
z_X	0.131(2)	0.135(2)
R_{Bragg}; R_f	18.3; 10.6	26.3; 23.0
R_{wp}; R_{expt}	2.75; 1.45	3.46; 1.29
χ^2	3.59	7.14

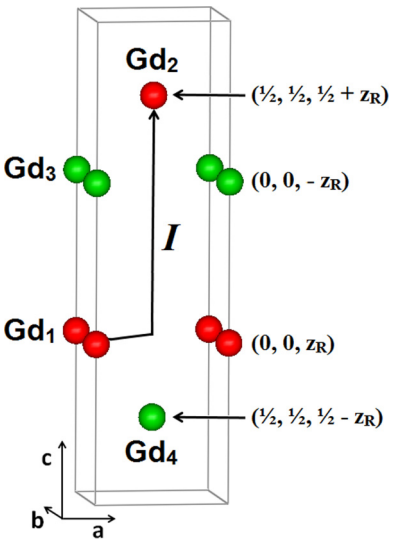

FIG. 3. (Color online) Representation of the two Gd sublattices in the CeScSi-type structure.

occupy the 4(e) (0,0,z_{Gd}), 4(c) (0,1/2,0), and 4(e) (0,0,z_X) crystallographic sites, respectively. The crystallographic unit cell contains four gadolinium atoms with positions (0,0,z_{Gd}), (1/2,1/2,1/2 + z_{Gd}), (0,0, − z_{Gd}), and (1/2,1/2,1/2 − z_{Gd}), which we label Gd_1, Gd_2, Gd_3, and Gd_4, respectively. These atoms are connected in pairs by the I-centering operation as shown in Fig. 3.

B. Magnetic structure of GdMgSn

The neutron powder diffraction pattern recorded at 5.4 K (Fig. 1) has many additional purely magnetic peaks. The upper panel of Fig. 4 shows the thermal variation of the intensity of the strongest magnetic diffraction peak of GdMgSn. The kink in the intensity at around 25 K suggests a change in the magnetic structure. Further evidence for a change in magnetic

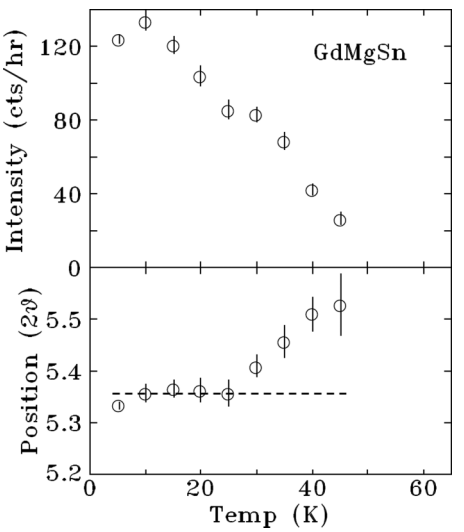

FIG. 4. Temperature dependence of the intensity (top) and of the 2θ position (bottom) of the strongest magnetic diffraction peak of GdMgSn.

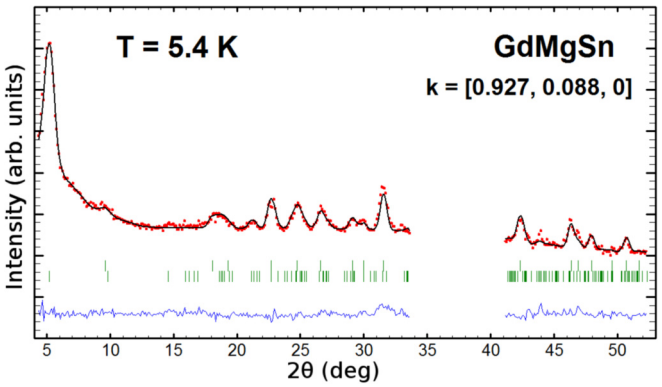

FIG. 5. (Color online) Refinement of the neutron powder diffraction pattern of GdMgSn recorded at 5.4 K with $\lambda = 1.3286(1)$ Å. The top row of Bragg markers corresponds to the nuclear contribution and the bottom row corresponds to the magnetic contribution.

structure comes from the position of this peak which clearly starts to move to higher angles above 25 K (lower panel of Fig. 4).

The diffraction pattern recorded at 5.4 K (Fig. 5) can be indexed by the propagation vector $\vec{k} = [\sim 0.93, \sim 0.09, 0]$, indicating an incommensurate antiferromagnetic structure. The absence of any contribution to the nuclear diffraction peaks immediately rules out a conical magnetic structure with cone angles other than 90°. Although the absence of higher-order harmonic peaks suggests that a square-wave-modulated magnetic structure can be excluded, the magnetic diffraction peaks corresponding to the first odd integer harmonic ($3k$) would be difficult to observe due to the low signal-to-noise ratio and the very weak amplitude expected for these magnetic peaks [i.e., $A(3k) = A(k)/3$].

The neutron diffraction pattern can be refined using either a planar helimagnetic structure (corresponding to a conical magnetic structure with a cone angle of 90°) or a sinusoidally modulated magnetic structure. When performing conical magnetic structure refinements with FULLPROF, no symmetry operations can be introduced (i.e., all of the magnetic atoms within a primitive unit cell must be given), meaning the magnetic refinements have to be performed using the $P\bar{1}$ magnetic space group. As a result, in order for the propagation vector $\vec{k}' = [q_x, q_y, 0]$ to remain within the first Brillouin zone, q_x and q_y are restricted: $q_x \leqslant 0.5$ and $q_y \leqslant 0.5$ [37]. However, to facilitate comparison with the magnetic structures previously reported for the CeScSi-type *R*MgSn and *R*MgPb compounds (refined with the magnetic space group $I\bar{1}$) [4,22], we have used the propagation vector $\vec{k} = [q_x, q_y, 0]$ with $q_x \leqslant 1$ and $q_y \leqslant 0.5$.

For the planar helimagnetic structure (flat spiral or cycloidal magnetic structure) [38], the magnetic moments are oriented in the ab plane ($\theta_n = 0°$) with a magnitude μ_{Gd} of $6.11(10)\mu_B$ (Table II). The planar orientation of the Gd^{3+} magnetic moments combined with the q_x and q_y components of the propagation vector give a cycloidal magnetic structure [38]. The magnetic moments of the alternative, sinusoidally modulated magnetic structure are also oriented in the ab plane with a sine-wave amplitude $A(k) = 8.53(14)\mu_B$, giving

TABLE II. Results from the various refinements of the 5.4 K $\lambda = 1.3286(1)$ Å neutron diffraction pattern of GdMgSn.

	Helimagnetic	Sinusoidal/square
a (Å)	4.389(3)	4.391(3)
c (Å)	15.851(11)	15.856(12)
z_{Gd}	0.339(1)	0.339(1)
z_{Sn}	0.131(2)	0.131(2)
q_x	0.927(4)	0.928(6)
q_y	0.088(4)	0.085(3)
Helimagnetic		
θ_c (deg)	90	
θ_n (deg)	0	
Magnetic phases (Gd_{1-4})	0; 0; 0.5; 0.5	
μ_{Gd} (units of μ_B)	6.11(10)	
Sinusoidal/Square		
$A(k)_{Gd}$		8.53(14)
θ (deg)		90
Magnetic phases (Gd_{1-4})		0; 0; 0.5; 0.5
μ_{Gd} (units of μ_B)		6.03(10)[a]/6.70(11)[b]
R_{Bragg}; R_f	19.6; 12.8	19.2; 12.6
R_{magn}	10.8	10.8
R_w; R_{expt}	2.91; 1.43	2.90; 1.43
χ^2	4.14	4.10

[a]Mean magnetic moment in the sine-modulated structure μ is calculated from the amplitude $A(k)$ with the relation $\mu = A(k)2^{-1/2}$.
[b]Mean magnetic moment in the square-modulated structure is calculated with the relation $\mu = A(k)\pi/4$.

a magnetic moment μ_{Gd} of $6.03(10)\mu_B$ (Table II). As q_y is almost equal to $1 - q_x$, ($q_x \sim q_y$ with the propagation vector $\vec{k}'$), the azimuthal angle ϕ (relative to the a axis) cannot be refined for either magnetic structure. Finally, the two magnetic structures lead to similar refinements and it is virtually impossible to distinguish between them on the basis of the various refinement R factors presented in Table II.

A further neutron diffraction pattern recorded at 5.4 K with a wavelength of $\lambda = 2.3731(1)$ Å confirms the absence of very low-angle magnetic diffraction peaks and the existence of a q_y component of the propagation vector (Fig. 6). The refinement

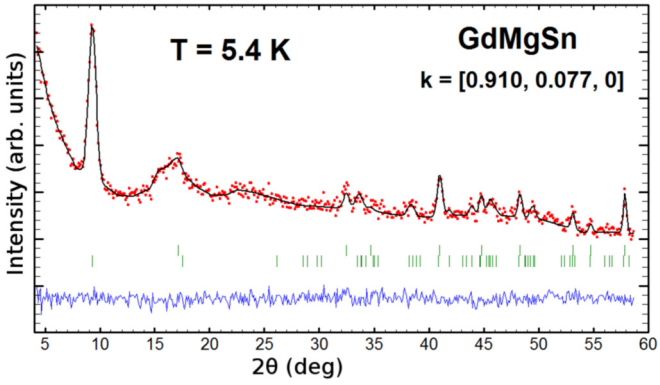

FIG. 6. (Color online) Refinement of the neutron powder diffraction pattern of GdMgSn recorded at 5.4 K with $\lambda = 2.3731$ Å. The top row of Bragg markers corresponds to the nuclear contribution and the bottom row corresponds to the magnetic contribution.

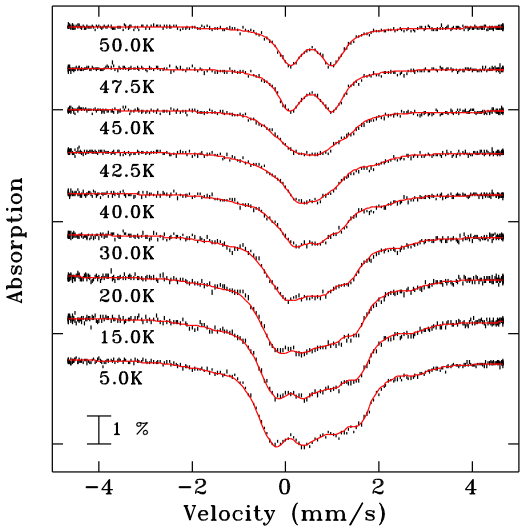

FIG. 7. (Color online) Fitted ^{155}Gd Mössbauer spectra of GdMgSn.

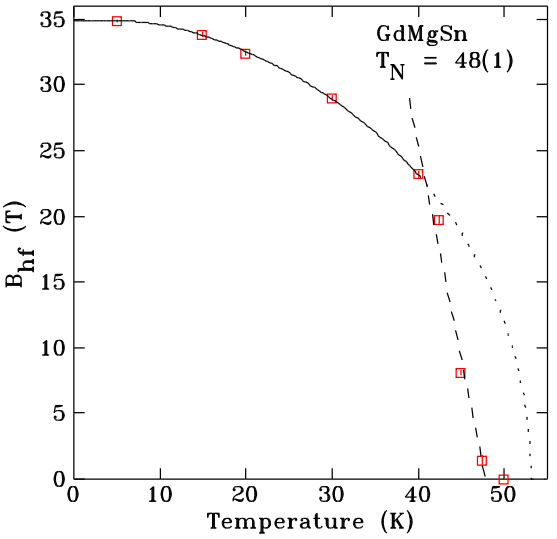

FIG. 8. (Color online) Temperature dependence of the hyperfine field ($B_{\rm hf}$) of GdMgSn with a single-site fit. The $J = 7/2$ Brillouin fit is shown by the solid black line between 5 and 40 K. The dotted line above 40 K shows the expected behavior of the hyperfine field, and the dashed line shows the actual behavior.

of this pattern considering the ab-plane cycloidal magnetic structure gives a propagation vector $\vec{k} = [0.910(2),0.077(2),0]$ and a magnetic moment of $\mu_{\rm Gd} = 6.54(16)\mu_{\rm B}$, which is relatively close to the free-ion value of $7.00\mu_{\rm B}$ expected for the Gd^{3+} ion. With this neutron wavelength, the magnetic diffraction peaks are extended on a broader angular range, allowing a more accurate determination of the q_x and q_y components of the propagation vector. Thus, the magnetic structure at 5.4 K will be described considering these q_x and q_y components of the propagation vector, which are slightly smaller than those refined with the neutron pattern recorded with $\lambda = 1.3286(1)$ Å.

There are now a total of three possible magnetic structures for GdMgSn: cycloidal, square-wave-modulated, and sine-wave modulated. We therefore turn to ^{155}Gd Mössbauer spectroscopy to help determine which of the competing magnetic structures is correct.

Gd occupies the 4e crystallographic site, which has 4mm point symmetry. This ensures an axially symmetric electric field gradient (EFG) tensor, with an asymmetry parameter $\eta = 0$ and the principal axis aligned with the crystallographic c axis [39]. Since the hyperfine field $B_{\rm hf}$ at the Gd site derives almost entirely from the local contribution of the Gd moment, $B_{\rm hf}$ will be parallel to the Gd moment, and so the angle (θ) between the principal axis of the EFG and $B_{\rm hf}$ is a direct measurement of the angle between the Gd moments and the crystallographic c axis.

The ^{155}Gd Mössbauer spectra of GdMgSn are shown in Fig. 7. Attempting to fit the 5 K spectrum with a sinusoidally varying hyperfine field yielded poor results, whereas a single-site fit was found to work quite well, and gives $\theta = 90^\circ$. This result is in agreement with the neutron diffraction results which indicate that the moments lie in the ab plane. As Mössbauer spectroscopy cannot distinguish between a moment pointing parallel or antiparallel to a given direction, a square-wave-modulated magnetic structure will appear as a single gadolinium environment. In addition, since $\eta = 0$, all azimuthal directions are equivalent. A cycloidal magnetic structure with the moments rotating in the ab plane is thus indistinguishable from a square-wave-modulated magnetic structure.

Figure 8 shows a clear break from the expected $J = 7/2$ Brillouin function at temperatures above 40 K, suggesting a magnetic transition. Between 40 K and $T_{\rm N} = 48(1)$ K, the spectra can be refined as either sine-wave modulated or single site. As the spectra in this temperature range are centrally peaked and have no defining features, the two types of fits are equally good. The hyperfine field found with the single-site fit corresponds to the average value of the hyperfine field distribution of the sine-wave fits.

The ^{155}Gd Mössbauer spectra allows exclusion of the sine-wave-modulated magnetic structure only at low temperatures, so a complementary method is needed. We therefore turn to our recent work on the calculation of ^{119}Sn hyperfine field distributions in RMgSn compounds to help determine the correct magnetic structure [40]. This method has successfully reproduced the major features seen by ^{119}Sn Mössbauer spectroscopy in other CeScSi-type RMgSn compounds with R = Nd, Tb, Dy, Ho, and Er. It was also able to discriminate between competing magnetic structure models proposed by neutron powder diffraction in the case of TbMgSn.

Tin does not have a magnetic moment so any hyperfine field observed by ^{119}Sn Mössbauer spectroscopy is induced by either an external applied magnetic field or a magnetic field produced by a neighboring atom. The method described in Ref. [40] uses the magnetic structure description obtained from neutron powder diffraction to calculate the expected transferred hyperfine field distribution at the Sn site in RMgSn compounds. The results of the calculations for the three candidate magnetic structures are shown in Figs. 9(a), 9(b), and 9(c) and are clearly distinct. The cycloidal structure yields a single peak—the Sn atoms experience a unique magnetic environment—while the square-wave-modulated magnetic

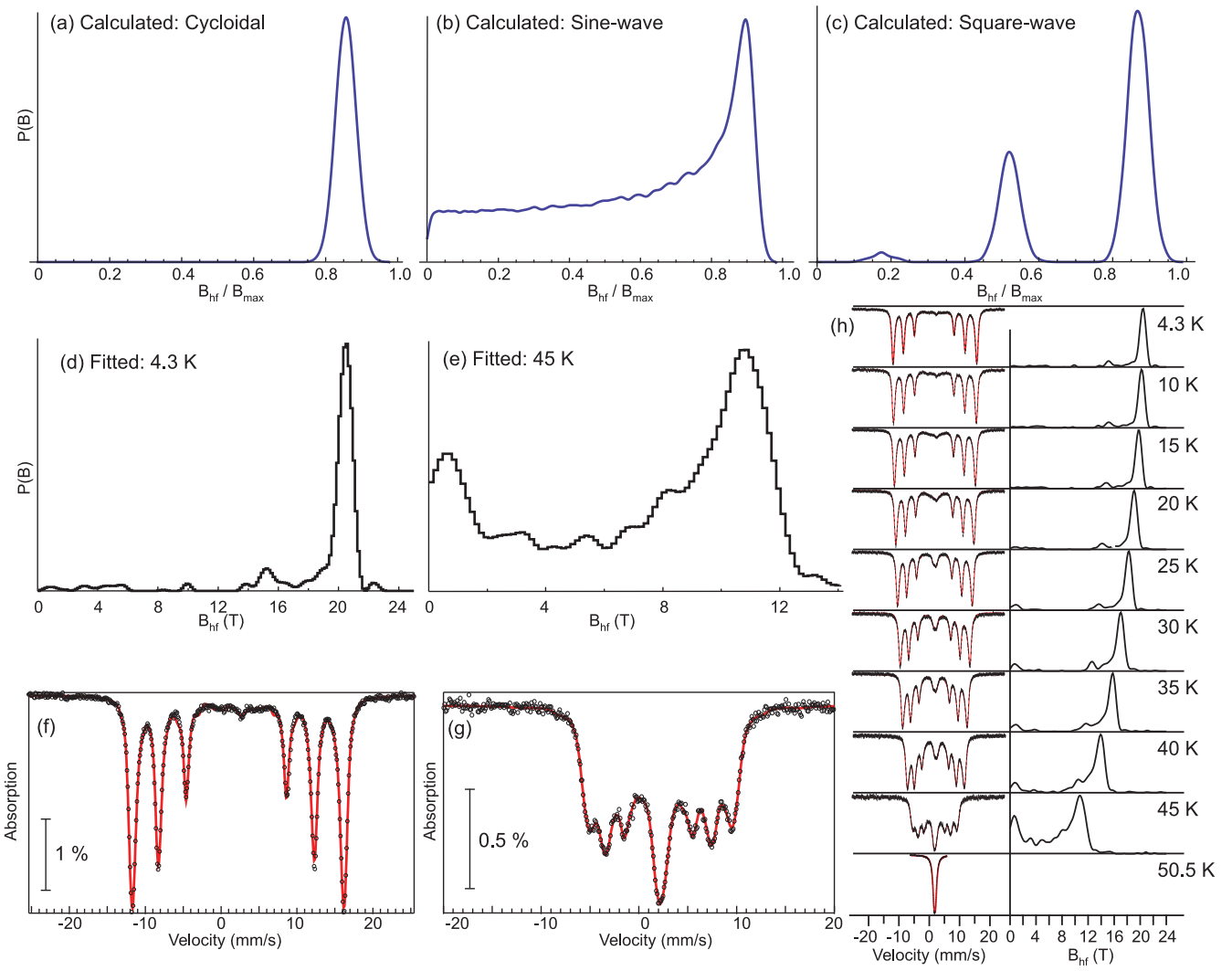

FIG. 9. (Color online) (a),(b),(c) Calculated transferred hyperfine field distribution (THFD) for the three possible magnetic structures. (d),(e) Fitted THFD of GdMgSn obtained from the ^{119}Sn Mössbauer spectra. (f),(g) ^{119}Sn Mössbauer spectra of GdMgSn and fit to the data (solid red line). (h) Temperature evolution of the ^{119}Sn Mössbauer spectra and THFD of GdMgSn between 4 and 45 K.

structure leads to three peaks with quite different intensities. Finally, the sine-wave-modulated magnetic structure shows a broad distribution of hyperfine fields in the form of a plateau leading to terminal peak.

The temperature evolution of the ^{119}Sn Mössbauer spectra and the corresponding hyperfine field probability distributions are shown in Fig. 9(h). Comparison of the calculated and measured hyperfine field distributions reveals that at low temperatures the Gd moments in GdMgSn adopt a cycloidal magnetic structure. Above 40 K the probability distribution changes to resemble that calculated for a sine-wave-modulated structure.

We note that an elliptical magnetic structure corresponding to both orientation and magnitude modulation cannot be excluded around 40 K. In fact, above 25 K the hyperfine field probability distributions in Fig. 9(h) have an additional feature around 2 T. Figure 4 also shows that the position of the strongest magnetic diffraction peak shifts above 25 K, indicating an evolution of the magnetic propagation vector. We therefore conclude that the magnetic structure of GdMgSn evolves from cycloidal (Fig. 10) at low temperatures to modulated at temperatures above 40 K by passing through an intermediate elliptical magnetic structure.

We also note that there is no one-to-one correspondence between the hyperfine field distribution calculated from Mössbauer spectra and a distribution of magnetic moments. This is because the hyperfine field distribution records the magnitude of the magnetic moments, making it impossible to directly retrieve the magnetic structure. While we cannot rule out more complex magnetic structures, the proposed ones are the simplest that are simultaneously consistent with neutron powder diffraction and ^{119}Sn and ^{155}Gd Mössbauer spectroscopy.

C. Magnetic structure of GdMgPb

The neutron powder diffraction pattern of GdMgPb recorded at 5.4 K (Fig. 11) shows many additional purely magnetic peaks that can be indexed by the propagation vector

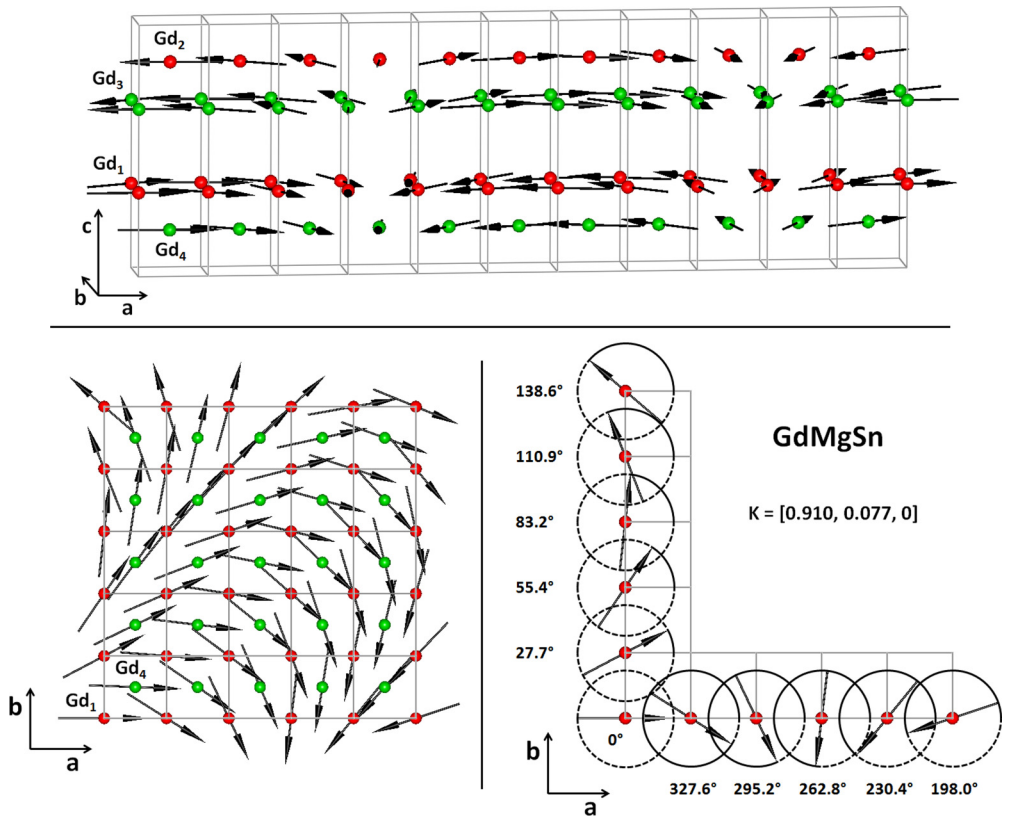

FIG. 10. (Color online) The cycloidal magnetic structure of GdMgSn at 5.4 K. For clarity, we have omitted the nonmagnetic Mg and Sn atoms.

$\vec{k} = [0.892,0,0]$, indicating an incommensurate antiferromagnetic structure.

The refinement of the difference between the neutron diffraction patterns recorded at 5.4 and 60 K using a cycloidal magnetic structure is shown in Fig. 12. As with GdMgSn, the neutron diffraction pattern can be refined using either a planar helimagnetic structure (flat spiral or cycloidal magnetic structure) or a sinusoidally or square-wave-modulated magnetic structure. Again the two magnetic structure models lead to refinements that are virtually impossible to distinguish (Table III).

For the planar helimagnetic structure (cone angle $\theta_c = 90°$), the magnetic moments are oriented in the ab plane (cycloidal magnetic structure) and have a magnitude μ_{Gd} of 5.26(12)μ_B (Table III). For the sinusoidally modulated magnetic structure the magnetic moments are also oriented in the ab plane with an azimuthal angle ϕ (relative to the a axis) of 41(7)° and an amplitude of the sine wave $A(k)$ of 7.46(17)μ_B, giving a mean magnetic moment μ_{Gd} of 5.28(12)μ_B and 5.86(13)μ_B for the

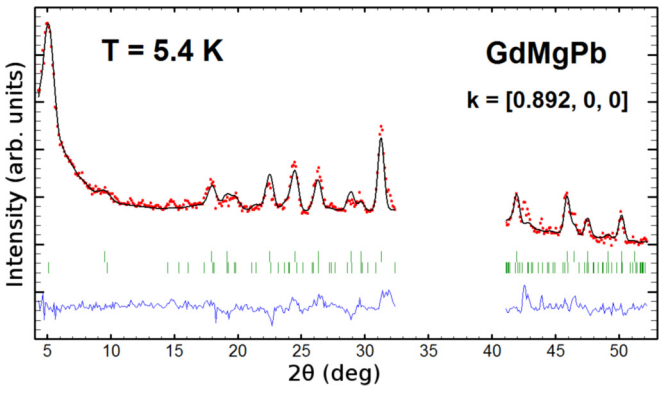

FIG. 11. (Color online) Refinement of the neutron powder diffraction pattern of GdMgPb recorded at 5.4 K with $\lambda = 1.3286$ Å. The top row of Bragg markers corresponds to the nuclear contribution and the bottom row corresponds to the magnetic contribution.

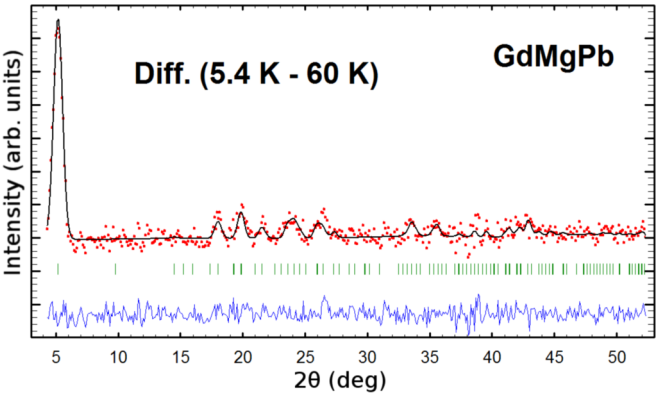

FIG. 12. (Color online) Refinement of the difference between the neutron powder diffraction patterns of GdMgPb recorded at 5.4 and 60 K with $\lambda = 1.3286$ Å. As all peaks are magnetic, the Bragg markers are for the magnetic phase.

TABLE III. Results from the various refinements of the 5.4 K neutron diffraction pattern of GdMgPb.

Parameter	Helimagnetic	Sinusoidal/square
a (Å)	4.430(4)	4.430(4)
c (Å)	15.978(14)	15.980(15)
z_{Gd}	0.342(1)	0.342(1)
z_{Pb}	0.135(2)	0.135(2)
q_x	0.892(4)	0.892(4)
Helimagnetic		
θ_c (deg)	90	
θ_n (deg)	0	
ϕ_n (deg)	0	
Magnetic phases (Gd_{1-4})	0; 0; 0.5; 0.5	
μ_{Gd} (units of μ_B)	5.26(12)	
Sinusoidal/square		
$A(k)_{Gd}$		7.46(17)
θ (deg)		90
ϕ (deg)		41(7)
Magnetic phases (Gd_{1-4})		0; 0; 0.5; 0.5
μ_{Gd} (units of μ_B)		5.28(12)[a]/5.86(13)[b]
R_{Bragg}; R_f	24.4; 17.7	24.5; 17.8
R_{magn}	15.5	15.8
R_{wp}; R_{expt}	3.54; 1.28	3.54; 1.28
χ^2	7.57	7.59

[a]Mean magnetic moment in the sine-modulated structure μ is calculated from the amplitude $A(k)$ with the relation $\mu = A(k)2^{-1/2}$.
[b]Mean magnetic moment in the square-modulated structure is calculated with the relation $\mu = A(k)\pi/4$.

sine-modulated and square-modulated structures, respectively (Table III). In both cases, the refined magnetic moment μ_{Gd} is smaller than the expected $7\mu_B$ for the Gd^{3+} free ion.

The ^{155}Gd Mössbauer spectra shown in Fig. 13 can be fitted with a single site from 5 K to $T_N = 49(1)$ K. This again allows us to exclude the sine-wave-modulated magnetic structure at low temperatures.

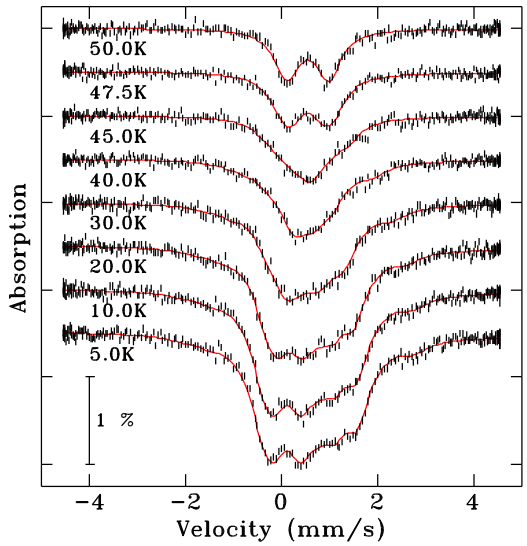

FIG. 13. (Color online) Fitted ^{155}Gd Mössbauer spectra of GdMgPb.

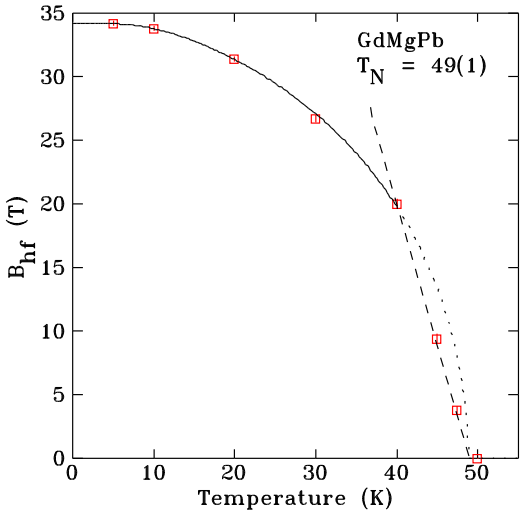

FIG. 14. (Color online) Temperature dependence of the hyperfine field (B_{hf}) of GdMgPb with a single-site fit. The $J = 7/2$ Brillouin fit is shown by the solid black line between 5 and 40 K. The dotted line above 40 K shows the expected behavior of the hyperfine field, and the dashed line shows the actual behavior.

B_{hf} is plotted in Fig. 14 and follows a $J = 7/2$ Brillouin function below 40 K and deviates from this trend above 40 K in the same manner that was seen for GdMgSn. We also note that the position of the strongest magnetic peak in the neutron diffraction patterns of GdMgPb (not shown) behaves similarly to that seen in Fig. 4 for GdMgSn. The position of the strongest magnetic peak gradually increases above 20 K, indicating that the magnetic propagation vector changes. As discussed in the Introduction, the magnetic structures of the CeScSi-type $RMgX$ (X = Sn,Pb) compounds tend to be similar for a given rare-earth element. Thus, given the strong similarities in both the behavior of the ^{155}Gd hyperfine fields and the magnetic structures found by neutron powder diffraction at 5.4 K, we conclude that both GdMgSn and GdMgPb adopt a cycloidal magnetic structure at low temperatures, pass through an intermediate elliptical structure between ~25 K and 40 K, and finally adopt a modulated magnetic structure between 40 K and T_N. To the best of our knowledge GdMgSn and GdMgPb are the first CeScSi-type compounds known to have this kind of magnetic structure transition.

IV. CONCLUSION

The CeScSi-type structure, magnetic ordering temperature, and antiferromagnetic behavior in GdMgSn and GdMgPb have been confirmed by both neutron powder diffraction and Mössbauer spectroscopy (^{119}Sn and ^{155}Gd). These complementary techniques reveal an incommensurate cycloidal magnetic structure at 5.4 K characterized by an ab-plane orientation of the magnetic moments and propagation vectors $\vec{k} = [0.910,0.077,0]$ and $\vec{k} = [0.892,0,0]$ for GdMgSn and GdMgPb, respectively. Similar magnetic structures have been reported for CeScSi-type ErZrSb [7] and TbMgSn [21]. Thus, GdMgSn and GdMgPb are the third and fourth CeScSi-type structure compounds reported to adopt incommensurate cycloidal magnetic structures. Above 40 K, a magnetic structure

transition is observed for both compounds and the cycloidal magnetic structure transforms to a modulated one, leading to an additional kind of magnetic structure transition in the CeScSi-type compounds.

ACKNOWLEDGMENTS

Financial support for various stages of this work was provided by the Natural Sciences and Engineering Research Council of Canada and Fonds Québécois de la Recherche sur la Nature et les Technologies. We thank J. M. Cadogan, UNSW Canberra, Australia, for many useful discussions. We gratefully acknowledge the assistance of Raghu Rao and Robert Speranzini in arranging for the activation of the ^{155}Gd Mössbauer source in the National Research Universal (NRU) research reactor, which is operated by Atomic Energy of Canada, Ltd., at Chalk River, Ontario.

[1] P. Manfrinetti, A. Provino, and K. A. Gschneidner, Jr., J. Alloys Compd. **482**, 81 (2009).
[2] A. Provino, K. A. Gschneidner, Jr., and P. Manfrinetti, J. Alloys Compd. **497**, 131 (2010).
[3] P. Lemoine, A. Vernière, J. F. Marêché, and B. Malaman, J. Alloys Compd. **508**, 9 (2010).
[4] P. Lemoine, A. Vernière, G. Venturini, J. F. Marêché, S. Capelli, and B. Malaman, J. Magn. Magn. Mater. **324**, 2937 (2012).
[5] S. Singh, S. K. Dhar, P. Manfrinetti, A. Palenzona, and D. Mazzone, J. Magn. Magn. Mater. **269**, 113 (2004).
[6] P. Manfrinetti, A. V. Morozkin, O. Isnard, P. Henry, and A. Palenzona, J. Alloys Compd. **450**, 86 (2008).
[7] A. V. Morozkin, K. Halich, R. Welter, and B. Ouladdiaf, J. Alloys Compd. **393**, 34 (2005).
[8] Y. Uwatoko, M. Kosaka, and T. Sigeoka, Physica B **259–261**, 114 (1999).
[9] S. A. Nikitin, I. A. Ovtchenkova, Yu. V. Skourski, and A. V. Morozkin, J. Alloys Compd. **345**, 50 (2002).
[10] S. Couillaud, E. Gaudin, V. Franco, A. Conde, R. Pöttgen, B. Heying, U. Ch. Rodewald, and B. Chevalier, Intermetallics **19**, 1573 (2011).
[11] T. Shigeoka, M. Yokoyama, M. Kosaka, Y. Uwatoko, M. Furugen, S. Ishida, and S. Asano, Physica B **281–282**, 96 (2000).
[12] J. M. Cadogan, D. H. Ryan, R. Gagnon, and C. J. Voyer, J. Appl. Phys. **97**, 10A916 (2005).
[13] J. M. Cadogan and D. H. Ryan, Solid State Phenom **170**, 282 (2011).
[14] S. Tencé, O. Isnard, E. Gaudin, and B. Chevalier, J. Alloys Compd. **560**, 195 (2013).
[15] R. Welter, A. V. Morozkin, and K. Halich, J. Magn. Magn. Mater. **257**, 44 (2003).
[16] I. A. Tskhadadze, V. V. Chernyshev, A. N. Streletskii, V. K. Portnoy, A. V. Leonov, I. A. Sviridov, I. V. Telegina, V. N. Verbetskii, Yu. D. Seropegin, and A. V. Morozkin, Mater. Res. Bull. **34**, 1773 (1999).
[17] R. Welter, A. Vernière, G. Venturini, and B. Malaman, J. Alloys Compd. **283**, 54 (1999).
[18] B. Tyszka and J. Szade, J. Alloys Compd. **354**, 64 (2003).
[19] T. I. Ivanova, M. V. Gavrilko, S. A. Nikitin, I. A. Ovchenkova, A. V. Morozkin, D. Badurski, and K. P. Skokov, J. Magn. Magn. Mater. **300**, e489 (2006).
[20] S. Tencé, E. Gaudin, O. Isnard, and B. Chevalier, J. Phys.: Condens. Matter **24**, 296002 (2012).
[21] C. Ritter, A. Provino, P. Manfrinetti, and K. A. Gschneidner, Jr., J. Alloys Compd. **509**, 9724 (2011).
[22] P. Lemoine, A. Vernière, G. Venturini, S. Capelli, and B. Malaman, J. Magn. Magn. Mater. **324**, 961 (2012).
[23] D. H. Ryan, J. M. Cadogan, C. J. Voyer, M. Napoletano, P. Riani, and L. M. D. Cranswick, Mod. Phys. Lett. B **24**, 1 (2010).
[24] M. Potter, H. Fritzsche, D. H. Ryan, and L. M. D. Cranswick, J. Appl. Crystallogr. **40**, 489 (2007).
[25] D. H. Ryan and L. M. D. Cranswick, J. Appl. Crystallogr. **41**, 198 (2008).
[26] C. J. Voyer, D. H. Ryan, J. M. Cadogan, L. M. D. Cranswick, M. Napoletano, P. Riani, and F. Canepa, J. Phys.: Condens. Matter **19**, 436205 (2007).
[27] J. M. Cadogan, D. H. Ryan, M. Napoletano, P. Riani, and L. M. D. Cranswick, J. Phys.: Condens. Matter **21**, 124201 (2009).
[28] D. H. Ryan, J. M. Cadogan, L. M. D. Cranswick, K. A. Gschneidner, Jr., V. K. Pecharsky, and Y. Mudryk, Phys. Rev. B **82**, 224405 (2010).
[29] D. H. Ryan, N. R. Lee-Hone, J. M. Cadogan, P. C. Canfield, and S. L. Bud'ko, J. Phys.: Condens. Matter **23**, 106003 (2011).
[30] P. Lemoine, J. M. Cadogan, D. H. Ryan, and M. Giovannini, J. Phys.: Condens. Matter **24**, 236004 (2012).
[31] N. R. Lee-Hone, P. Lemoine, D. H. Ryan, A. Vernière, and B. Malaman, J. Appl. Phys. **113**, 17E107 (2013).
[32] J. Rodríguez-Carvajal, Physica B **192**, 55 (1993).
[33] T. Roisnel and J. Rodríguez-Carvajal, Mater. Sci. Forum **378–381**, 118 (2001).
[34] J. E. Lynn and P. A. Seeger, At. Data Nucl. Data Tables **44**, 191 (1990).
[35] C. J. Voyer and D. H. Ryan, Hyperfine Interact. **170**, 91 (2006).
[36] G. Le Caër and J. M. Dubois, J. Phys. E **12**, 1083 (1979).
[37] J. Rossat-Mignod, in *Neutron Scattering, Methods in Experimental Physics*, Vol. 23, Part C, edited by K. Sköld and D. L. Price (Academic Press, New York, 1987), p. 121.
[38] J. Rodríguez-Carvajal and F. Bourée, EPJ Web Conf **22**, 00010 (2012).
[39] G. A. Stewart, Mater. Forum **18**, 177 (1994).
[40] N. R. Lee-Hone, P. Lemoine, D. H. Ryan, B. Malaman, A. Vernière, and G. Le Caër, Hyperfine Interact. **226**, 309 (2014).